

THE IONOSPHERE AS A MEASURE OF SOLAR ACTIVITY

By M. L. Phillips

I. Introduction. Parallelism of Ionospheric and Solar Phenomena.

The long-period variation of ionospheric critical frequencies has long been known to parallel that of many solar and terrestrial phenomena, - the prevalence of sunspots, solar flocculi, auroral displays, variations in geomagnetism - all of which vary causally with solar activity. (See "Trends of Characteristics of the Ionosphere for Half a Sunspot Cycle," N. Smith, T.R. Gilliland, S.S. Kirby, J. Res. National Bureau of Standards, 21, 835; 1933 (RP1159). As examples of this co-variance, Figs. 1, 2, 3, and 4 herewith present the time trends manifested by the noon values of critical frequencies of the F2, F1, and E layers of the ionosphere, as well as the midnight values of the F2-layer critical frequency, as observed, respectively, at Washington, D.C., Slough, England, Huancayo, Peru, and Watheroo, W. Australia, while Fig. 5 presents values of relative sunspot number for the same time. Solid-line curves, in all cases, represent twelve-month-running-average values, while discrete points and dotted lines represent monthly values.

Comparison of the ionospheric time trends with that of the sunspot number shows several important facts:

(a) There exists long-period, but not short-period, parallelism between the twelve-month running averages of critical frequency and the sunspot number.

The striking long-period parallelism with sunspot number, which has been found to exist individually, but with varying proportionality, for all locations and all times, is important, since it enables the world-wide prediction of useful radio frequencies to be made for indefinitely long periods of time in advance. This follows from the fact that sunspots have been observed regularly for a long time (Cf. IRPL-R23, Solar-Cycle Data for Correlation with Radio Propagation Phenomena), and their trends are sufficiently well known to be predicted with a fair amount of accuracy. (Cf. IRPL-R25, "The Prediction of Solar Activity as a Basis for the Prediction of Radio Propagation Phenomena.").

Lack of accurate short-period parallelism may result for several reasons. Basically, sunspot number and critical frequency are co-causal, so that it should not be expected that short-period variations, which may be the result of statistical variation or the modifying effects of variable factors other than solar activity, should be closely

correlated. Besides this, the process of taking a twelve-month-running-average, which serves to remove seasonal variation as well as smooth the time trend of ionospheric data, serves only to smooth the sunspot-number time trend, and may be an erroneous index of short-period activity should the series of sunspot numbers possess a fairly short periodicity which is not an exact multiple of twelve months.

(b) The relative change of ionospheric critical frequency with sunspot number varies with layer, geographical location, and time of day.

In general, the amount of this variation increases with the magnitude of the quantity under consideration, greater variation throughout the solar cycle being manifest for $f^{\circ}F_2$ than for $f^{\circ}E$, for example, and greater variation for noon than for midnight $f^{\circ}F_2$, in temperate latitudes.

(c) Magnitude of the seasonal variation generally varies with the quantity under consideration.

This may be noted in the diminishing size of the seasonal oscillations of all critical frequencies about their twelve-month-running-average values with the approach of sunspot minimum, and in the progressively greater seasonal oscillation of the E-, F1-, and F2-layer critical frequencies.

(d) The twelve-month running-average curves of critical frequency are smoother than those for sunspot number.

This suggests that ionospheric measurements of critical frequencies, being fairly continuous, and far less erratic than the appearance of sunspots, may be a considerably better index of fundamental solar activity than sunspot numbers.

II. Correlation of Critical Frequencies and Sunspot Number

The correlation between ionospheric critical frequency and sunspot number is approximately linear, for all layers, all times of day, and all geographical locations. This is shown by Figs. 6, 7, 8, and 9, which show the variation of twelve-month running-average critical frequency, observed at Washington, D.C., plotted against the twelve-month running-average sunspot number throughout the past solar cycle, for the E-, F1-, and F2-layers at noon, as well as the pre-sunrise minimum value for the F2-layer. The increased variation of critical frequency with sunspot number for greater magnitudes of critical frequencies, mentioned in (b), above, is more readily apparent here than in the previous time-trend curves. The very good correlation shown is most remarkable when one considers the highly arbitrary nature of the relative sunspot number, (the sum of the total sunspot count plus ten times the number of spot groups, all multiplied by a constant characteristic of observatory apparatus and seeing conditions), chosen by R. Wolf nearly a century ago as an index of solar activity. ("Mitteilungen über die Sonnenflecken," Naturforschende Gesellschaft in Zurich Vierteljahrsschrift, 1856-1865).

It is particularly interesting that the general linearity of this relationship between critical frequency and sunspot number parallels the linear relationship found by E. Pettit (Astrophys. J. April 1932, p.185) over a period of seven years, between solar emission of ultraviolet light and the number of sunspot groups. During one short period, somewhat better agreement was shown between ultraviolet light emission and the prevalence of Ca- and bright H-flocculi, thus suggesting the possibility of these serving as emission centers. A more probable explanation, suggested by Pettit, lies in the variable absorption of ultraviolet light by the solar atmosphere, this variation possibly depending upon the original ultraviolet emission.

Slopes of the linear trend curves of Figs. 6, 7, 8, and 9 indicate (as do similar trend curves for other times and places) values of solar activity, for the creation of ionospheric layers, which lie far below that for the creation of sunspots.

The ratio of the average critical frequency for any month to the twelve-month running-average value centered at that month, is, in all cases, nearly constant for any given month and location, although sometimes showing a slight correlation, probably linear, with sunspot number. (Cf. IRPL-R4, "Methods Used by IRPL for the Prediction of Ionosphere Characteristics and Maximum Usable Frequencies"). The constancy of this monthly index is manifest in the time trends of Figs. 1, 2, 3, and 4 in which, as noted in (c) above, the magnitude of seasonal variation generally diminishes with sunspot number.

Because of the linearity of relationship between critical frequency and sunspot number, and because of the approximate constancy of monthly index, the variation of critical frequency of any ionospheric layer, at any location, may be expressed as

$$f^{\circ} = A \left[f_1(t) + S \left[f_2(t) \right] \right] \quad (1)$$

where A is the monthly index (ratio of monthly-average critical frequency to the twelve-month running-average centered at that month), t is the time of day, $f_1(t)$ the diurnal variation of the zero-sunspot intercepts of trend curves such as Figs. 6, 7, 8, and 9 (i.e., the value of f° for a sunspot number of zero), S the sunspot number, and $f_2(t)$ the diurnal variation of the slopes of trend curves such as those of Figs. 6, 7, 8, and 9.

This relationship enables very condensed nomographic presentation of the correlated ionospheric observations at any location. Detailed description of this method was presented in the report IRPL-R11, "A Nomographic Method for Both Prediction and Observation Correlation of Ionosphere Characteristics." Nomographic correlation of yearly average $f^{\circ}F2$ for the three long-established ionospheric stations of Washington, D.C., Huancayo, Peru, and Watheroo, W. Australia are presented in Figs. 10, 11, and 12. (In these cases, the value of A in the above equation is unity).

Figs. 13 through 48 present correlation of monthly average $f^{\circ}F2$ with sunspot number for each month of the year at the same stations.

Since sunspot numbers are roughly predictable, these nomograms not only furnish a complete survey of $f^{\circ}F2$ correlation with solar activity at these locations, but may also be used to predict future values of $f^{\circ}F2$.

If smoothed sunspot numbers are used, for any time, values thus determined from the nomograms may be used for comparison with individual measurements of $f^{\circ}F2$ at the same time, in order to determine their approximation to normality with respect to all data previously taken.

The locus of points forming the diurnal time scale for corresponding nomograms (not shown here) correlating E- and F1-layer critical frequencies with sunspot number, lies, in all cases, along a straight line, originating at $f^{\circ} = 0$ and extending diagonally to meet the sunspot-number scale at a value far below $S = 0$, and identical for all seasons - the threshold value of solar activity, expressed in "sunspot number", for the creation of the ionospheric layer at that location. If the value of this intercept is represented by B, Eq. (1) above may be expressed more simply for these layers, as

$$f^{\circ} = A f_3(t) (S \dagger B) \quad (2)$$

Values of B for $f^{\circ}E$ at Fairbanks, Alaska; Washington, D.C.; Hancayo, Peru; and Watheroo, W. Australia; are, respectively, 996, 574, 460, and 401. For $f^{\circ}F1$, the respective values of B are 468 (rather poorly determined), 766, 358, and 347.

For most locations and seasons, the locus of points determining the F2-layer diurnal time-scale is a loop, which is nearly collapsed into a straight line, and therefore, although accurately represented by Eq.(1), the $f^{\circ}F2$ may be approximately represented by the simpler Eq.(2). Washington, D.C. exhibits good approximate relationship of this sort for most months of the year, values of B for the various months, beginning with January, being approximately 109, 113, 109, 108, 93, 94, 93, 97, 112, 113, 115, and 116, and B for the yearly average being 111. Greatest departure from this approximation occurs during summer months, apparently being associated with slow ionic recombination with increased atmospheric temperature.

At Watheroo, W. Australia, the F2-layer diurnal time-scale loop better approximates a straight line at all seasons than at Washington, D.C., but indicates a residual ionization, independent of sunspot number, in that the intersection of the approximate line of the time scale with the $f^{\circ}F2$ scale is not at its zero point. Thus, in this case, a better approximation than Eq.(2) is given by the expression

$$f^{\circ}F2 = C \equiv A f_4(t) (S \dagger B) \quad (3)$$

Both B and C vary seasonally. Values of B for each month, beginning with January, are approximately 75, 77, 75, 84, 102, 102, 84, 84, 64,

61, 62, 66, with 76 being the corresponding value for the yearly average $f^{\circ}F2$. Values of C for each month, beginning with January, are approximately 1.8, 1.6, 1.6, 1.35, 0.85, 0.6, 1.4, 1.3, 1.9, 2.1, 2.15, and 2.2 Mc, with 1.65 Mc for the yearly average of $f^{\circ}F2$.

The diurnal time scales for locations near the auroral zones and near the geomagnetic equator generally do not approximate such simple straight-line relationships. Auroral-zone values are not known with extreme precision and are not presented here, but generally display a fairly close clustering of the points on the time scale, for all hours of the day. The nomograms for Huancayo, Peru, presented here, are typical of variations at the geomagnetic equator. Here the diurnal time scale is nearly vertical for most months. This may roughly be expressed as

$$f^{\circ}F2 = A f_5(t) \dagger DS + E \quad (4)$$

With increasing departure of the solar declination from the latitude of Huancayo, Peru, the time scale assumes the "figure-eight" form shown for June, in Fig. 30. During the hours represented fairly well by the straight-line portions of this time scale, the relation of $f^{\circ}F2$ to S is that of Eq. (3), the varying slopes of different parts of the time scale representing widely varying values of B and C .

III. Application of Ionospheric Data to Measurement of Solar Activity.

Both the generally good correlation between sunspot number and critical frequency, and the greater smoothness of critical frequency variations, indicate that ionospheric measurements may be the most reliable measure of solar activity available. The reliability of their use in this respect necessitates that data be used only from stations where a long series of measurements are available, and that the critical frequencies selected for such use possess maximum solar-activity variation with respect to random day-to-day variation or sensitivity to abnormal effects, such as those of ionospheric storminess.

Data from the three stations for which nomograms are here presented - Washington, D.C., Huancayo, Peru, and Watheroo, W. Australia - are available for all hours of the day over the longest time periods, the first station possessing a series of data beginning in 1933.

Figs. 49 and 50 illustrate the daily variability in each of the three ionospheric layers, for three typical seasons, for the stations Huancayo and Watheroo. It is seen that daily variability is least in the E layer, and greatest in the F2 layer, where night values frequently show less variation than day values. The E layer is, moreover, least subject to the effects of ionospheric storminess. Inspection of the data of Figs. 6, 7, 8, and 9, however, shows that there is far less variation of $f^{\circ}E$, $f^{\circ}F1$ and night $f^{\circ}F2$ values with solar activity than for daytime values of $f^{\circ}F2$. Because of the greater ratio of solar-activity variation to daily variation for daytime values of $f^{\circ}F2$, these, therefore, are the best for the estimation of solar activity.

On the nomograms of Figs. 13 through 48, the distance of any point of the diurnal time scale from the $f^{\circ}F2$ scale is a measure of the variation of $f^{\circ}F2$ with solar activity at the corresponding time of day. Those hours, designated on the time scale, which are farthest removed from the $f^{\circ}F2$ scale, are thus the best for use in estimating solar activity. Generally, these are hours near midday. The average "sunspot number" obtained by using $f^{\circ}F2$ values for several such hours, for all three stations, affords a fairly good index of solar activity, as is shown by the data of Table 1, where values for all hours of the day are presented, to show the relative unreliability achieved by the inclusion of values estimated from $f^{\circ}F2$ for night hours, and by the data of Fig. 51, where ionospheric "sunspot numbers" derived from the values of $f^{\circ}F2$ for the hours from 1000 to 1400, inclusive, are compared with Zurich sunspot numbers.

It may be noted that the departure of monthly-average Zurich sunspot numbers from the twelve-month running-average curve is, in general, greater than that of the monthly-average ionospheric index of solar activity. Moreover, (although this may be fortuitous), had the ionospheric index been used, conditions of minimum solar activity reached near the end of 1944 and the beginning of 1945 would have been anticipated by the generally low values given in the autumn of 1944. Consideration of the count, areas, or latitudes of sunspots and flocculi gave little assurance that the minimum of solar activity had been passed until more than a half year later.

The daily variability of sunspot count is considerably greater than that of ionospheric critical frequencies during the daytime. Even greater variability in the former ensues from the variability of seeing conditions, if the results of only a few observatories are used. This is illustrated by Fig. 52, which presents a mass plot of the relative sunspot numbers from the group of American observers whose data are issued regularly by the Department of Terrestrial Magnetism, Carnegie Institution of Washington. It may be noted that the spread of these points is considerably greater than that for the "sunspot numbers" determined from ionospheric data, as shown in Fig. 51.

Results of particularly reliable observers, whose observatory constants have been determined over a long period of time, however, may be better correlated, as may be seen from Fig. 53. In comparing the data of Figs. 52 and 53, with those of Fig. 51, however, it must be borne in mind that the former represent different measurements of the same quantity, whereas the data of Fig. 51 are measurements of different quantities, geographically far apart, and, therefore, more likely to vary.

IV. Conclusions

Accuracy in the estimation of future solar activity is of paramount importance in the prediction of usable radio frequencies, since the process of prediction consists of the application of all estab-

lished ionospheric trends to a predicted value of solar activity. Inasmuch as greater consistency is apparent in the estimate of solar activity from ionospheric data, from which a fair current estimate is ordinarily possible from only a few days' observations, the use of ionospheric data is of value both to complement and to extend existing knowledge of solar activity variations for correlation with numerous terrestrial phenomena.

Table 1 (continued)

Hour	Jan.	Feb.	Mar.	Apr.	May	June	July	Aug.
75 ^{OW}								
	<u>Huancayo, Peru</u>							
00	10	18	37	32	43	50	52	36
01	16	15	32	18	32	41	39	30
02	25	28	29	4	26	51	35	41
03	15	22	19	20	17	50	22	22
04	27	11	8	11	21	43	27	14
05	33	-6	-2	19	15	35	28	18
06	39	17	10	23	8	45	31	19
07	28	22	27	33	22	48	40	34
08	28	32	18	29	30	49	40	34
09	33	33	22	29	30	41	41	29
10	36	37	22	16	34	36	34	20
11	33	38	20	13	34	36	37	23
12	18	36	22	17	27	32	29	18
13	15	40	24	10	36	29	30	17
14	11	46	18	8	36	23	32	20
15	12	49	21	14	32	31	33	23
16	13	50	28	24	26	24	32	14
17	11	48	24	32	29	34	28	26
18	16	44	25	36	36	39	38	32
19	8	41	28	40	38	37	33	13
20	22	54	25	40	40	47	33	12
21	10	69	31	62	57	59	52	23
22	-1	62	32	47	49	55	44	39
23	9	61	30	38	39	48	45	40

Table 1 (continued)

Hour	Jan.	Feb.	Mar.	Apr.	May	June	July	Aug.
75 ⁰ N	Watheroo, W. Australia							
00	25	16	24	40	51	40	56	32
01	21	21	22	38	59	39	62	43
02	20	27	23	45	59	41	59	43
03	17	35	24	43	73	52	77	59
04	11	26	24	31	68	39	59	55
05	18	27	24	33	75	42	63	67
06	23	33	25	19	30	32	39	58
07	26	34	29	28	45	40	46	43
08	29	32	23	30	35	34	39	35
09	28	26	21	26	29	34	36	35
10	26	26	24	27	32	37	44	31
11	28	26	22	25	29	38	40	32
12	28	33	20	24	26	32	29	26
13	36	37	24	23	28	39	35	28
14	40	35	20	23	27	40	40	29
15	35	45	18	19	25	33	41	30
16	32	35	21	14	18	35	38	29
17	33	36	24	12	19	28	32	23
18	23	35	21	13	25	23	23	31
19	17	33	20	9	23	17	36	32
20	23	34	21	14	33	14	29	15
21	23	24	16	19	39	26	47	23
22	22	18	21	32	46	27	50	24
23	20	18	24	37	39	27	55	24

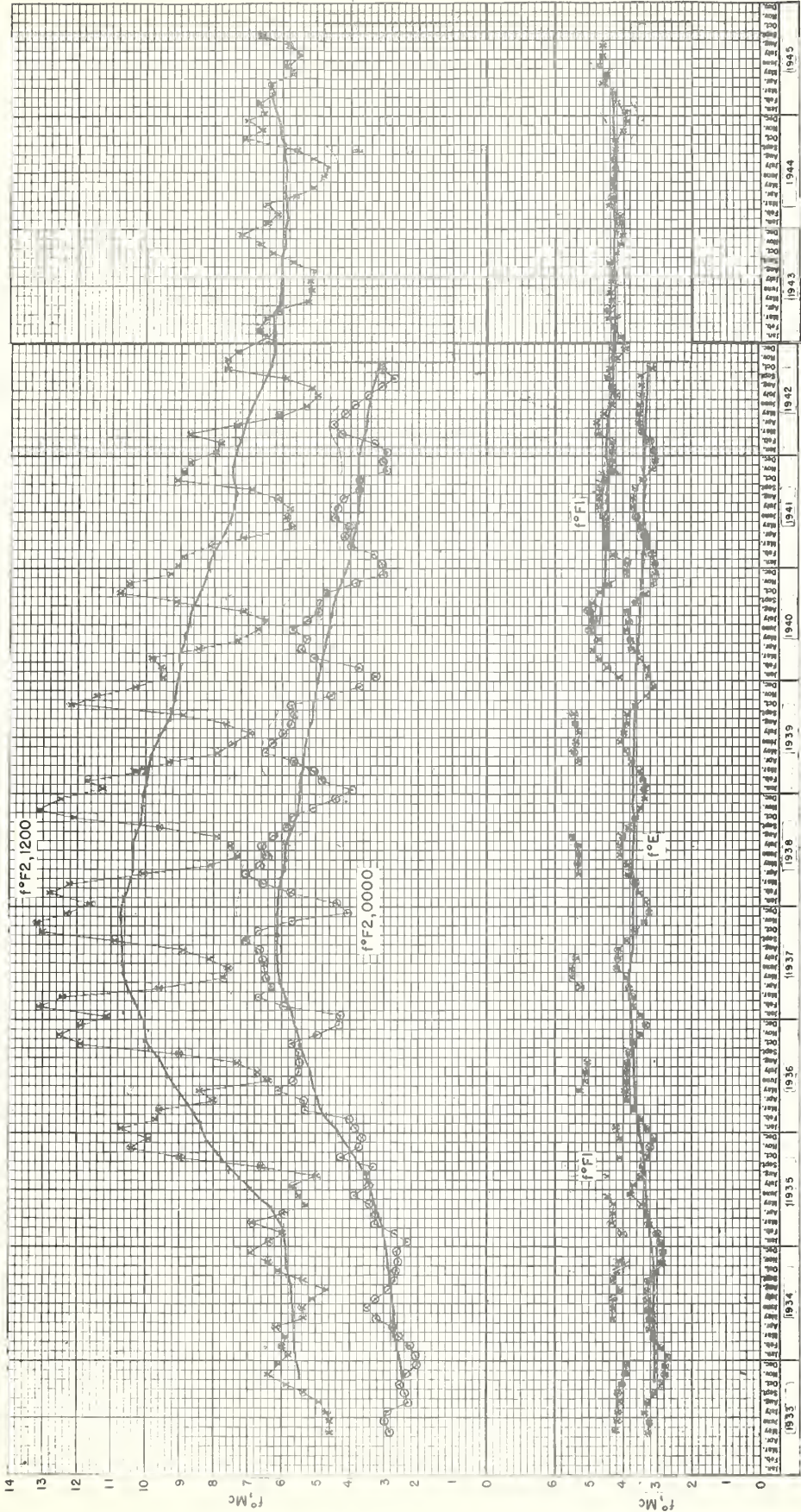


Fig. 1. TIME VARIATION OF NOON $f^{\circ}E$, $f^{\circ}F1$, $f^{\circ}F2$, AND MIDNIGHT $f^{\circ}F2$, AT WASHINGTON, D.C.

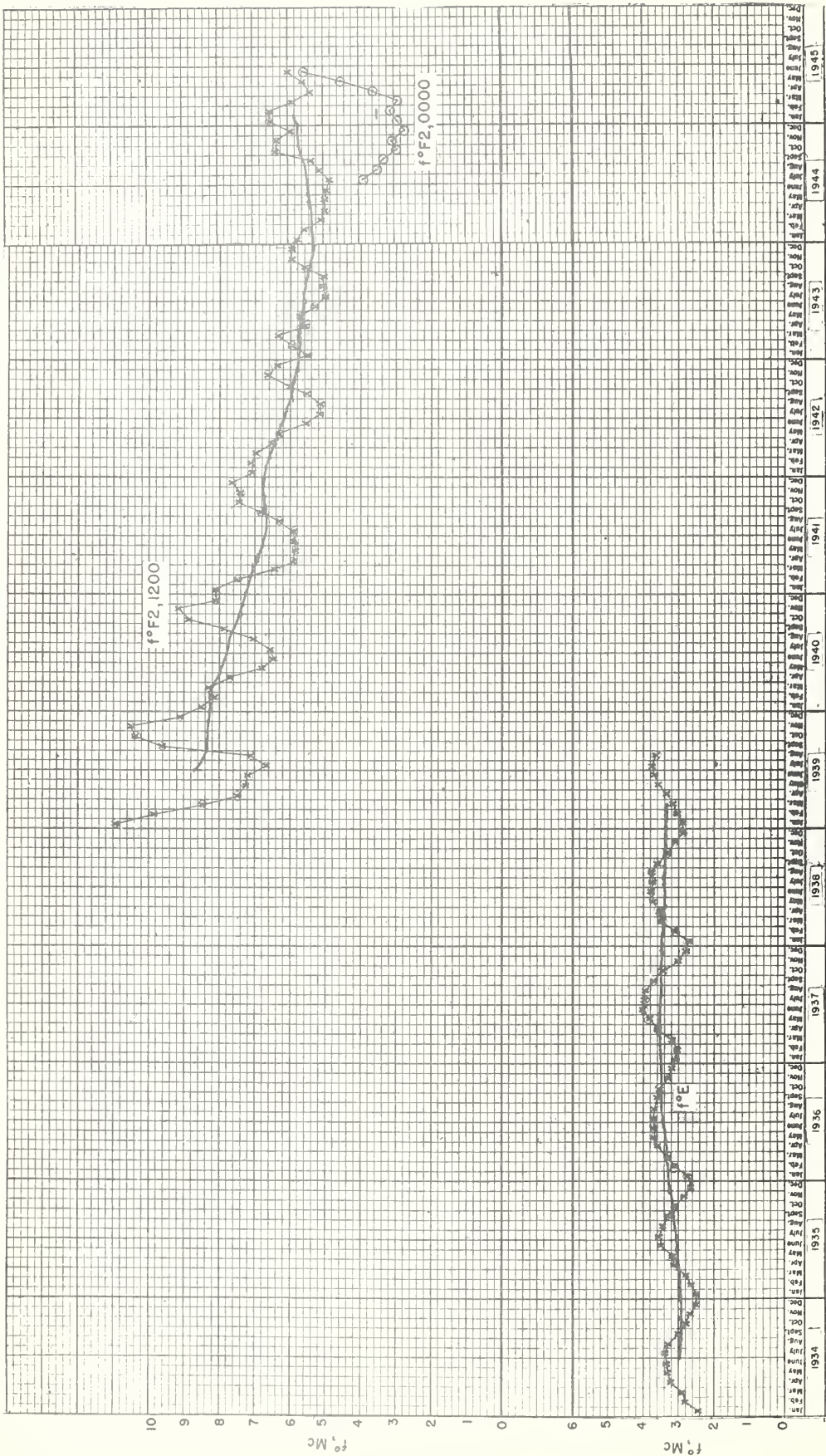


Fig. 2. TIME VARIATION OF NOON $f^{\circ}E$, $f^{\circ}F2$, AND MIDNIGHT $f^{\circ}F2$, AT SLOUGH, ENGLAND.

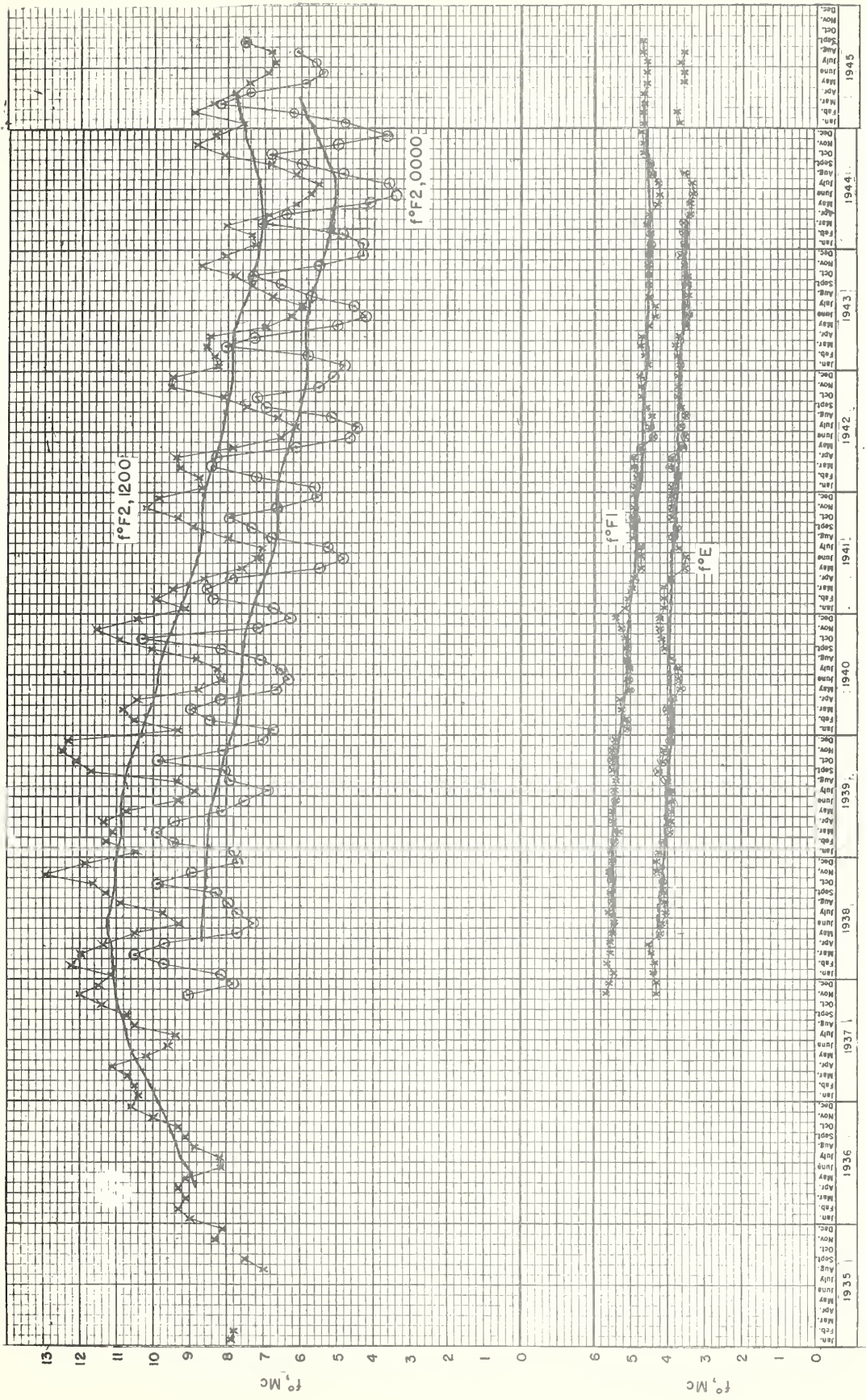


Fig. 3. TIME VARIATION OF NOON $f^{\circ}E$, $f^{\circ}F1$, $f^{\circ}F2$, AND MIDNIGHT $f^{\circ}F2$, AT HUANCAYO, PERU.

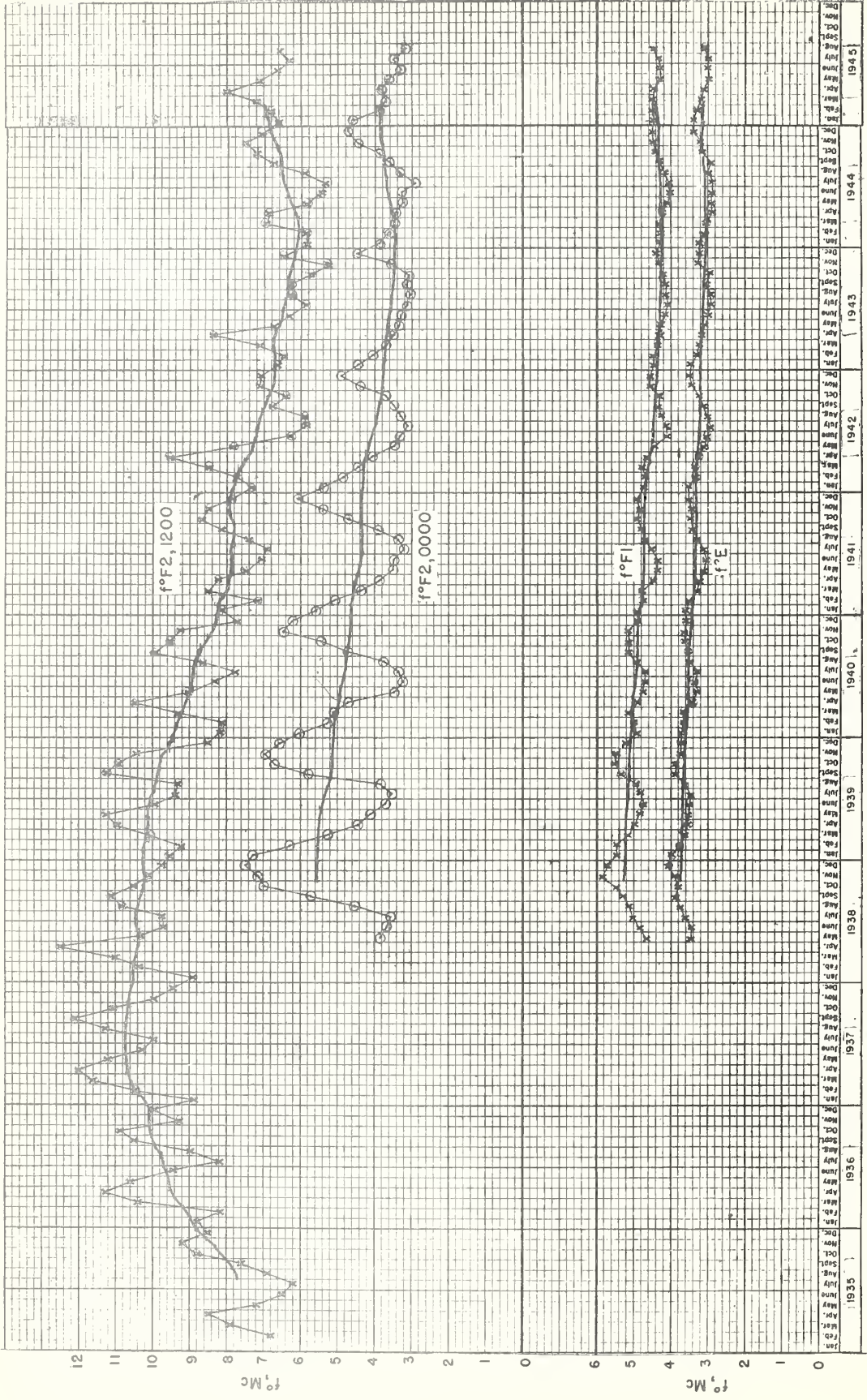


Fig. 4. TIME VARIATION OF NOON $f^{\circ}E$, $f^{\circ}F_1$, $f^{\circ}F_2$, AND MIDNIGHT $f^{\circ}F_2$, AT WATHEROO, W. AUSTRALIA.

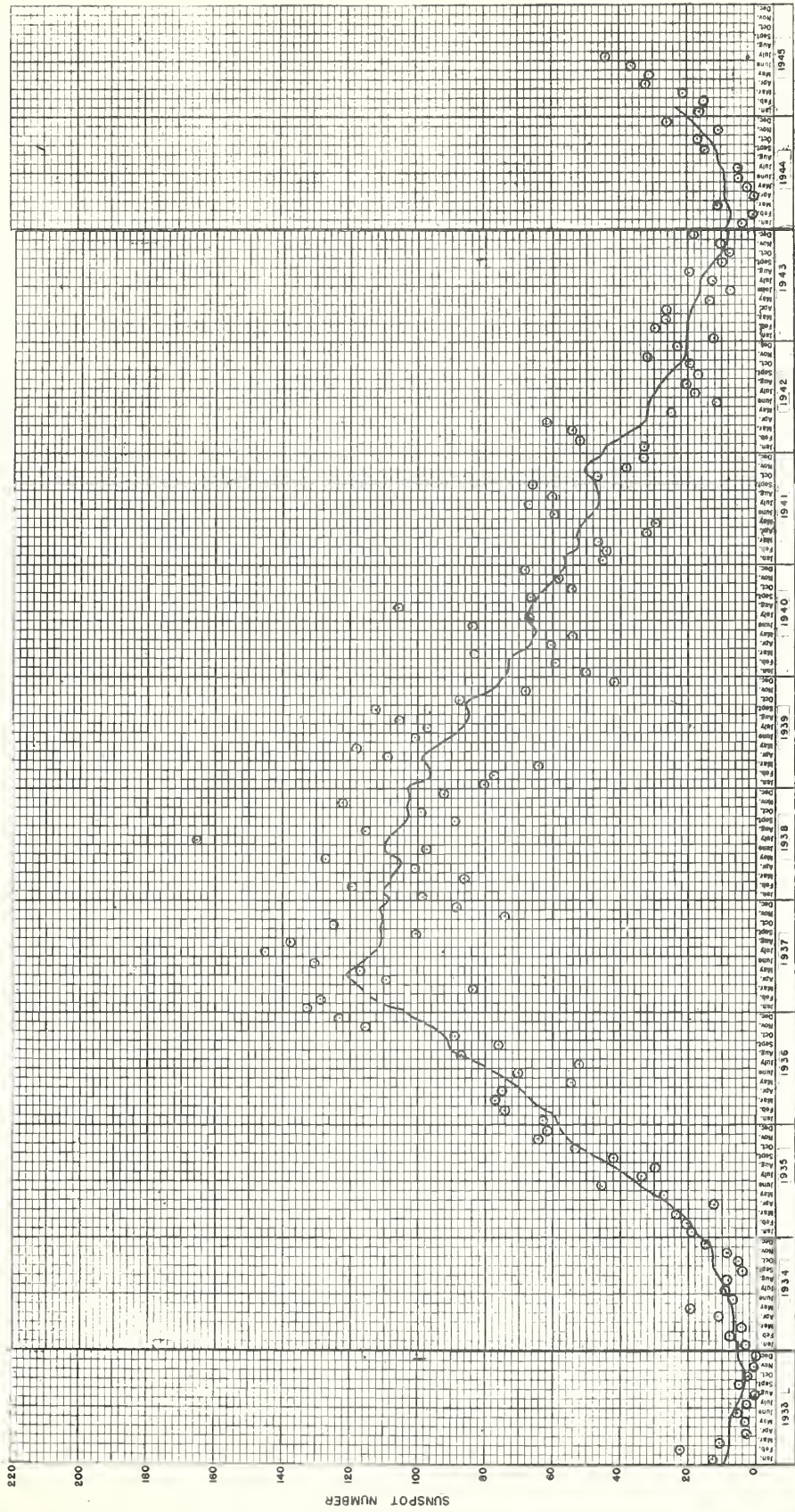


Fig. 5 TIME VARIATION OF RELATIVE SUNSPOT NUMBERS. (SOLID LINE REPRESENTS TWELVE-MONTH RUNNING-AVERAGE VALUES)

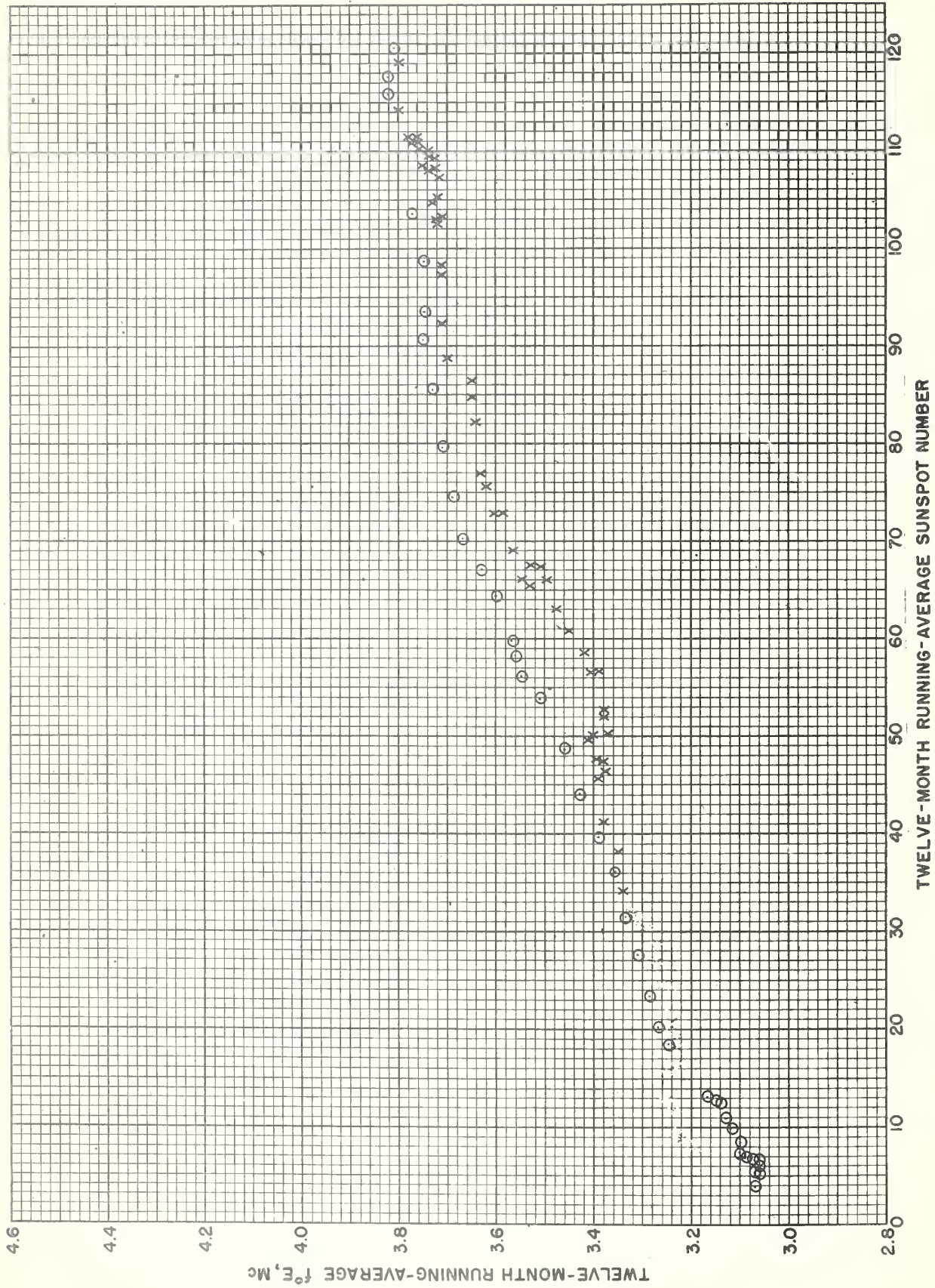


Fig. 6. VARIATION OF TWELVE-MONTH RUNNING-AVERAGE f°E, 1200, AT WASHINGTON, D.C., WITH TWELVE-MONTH RUNNING-AVERAGE SUNSPOT NUMBER.

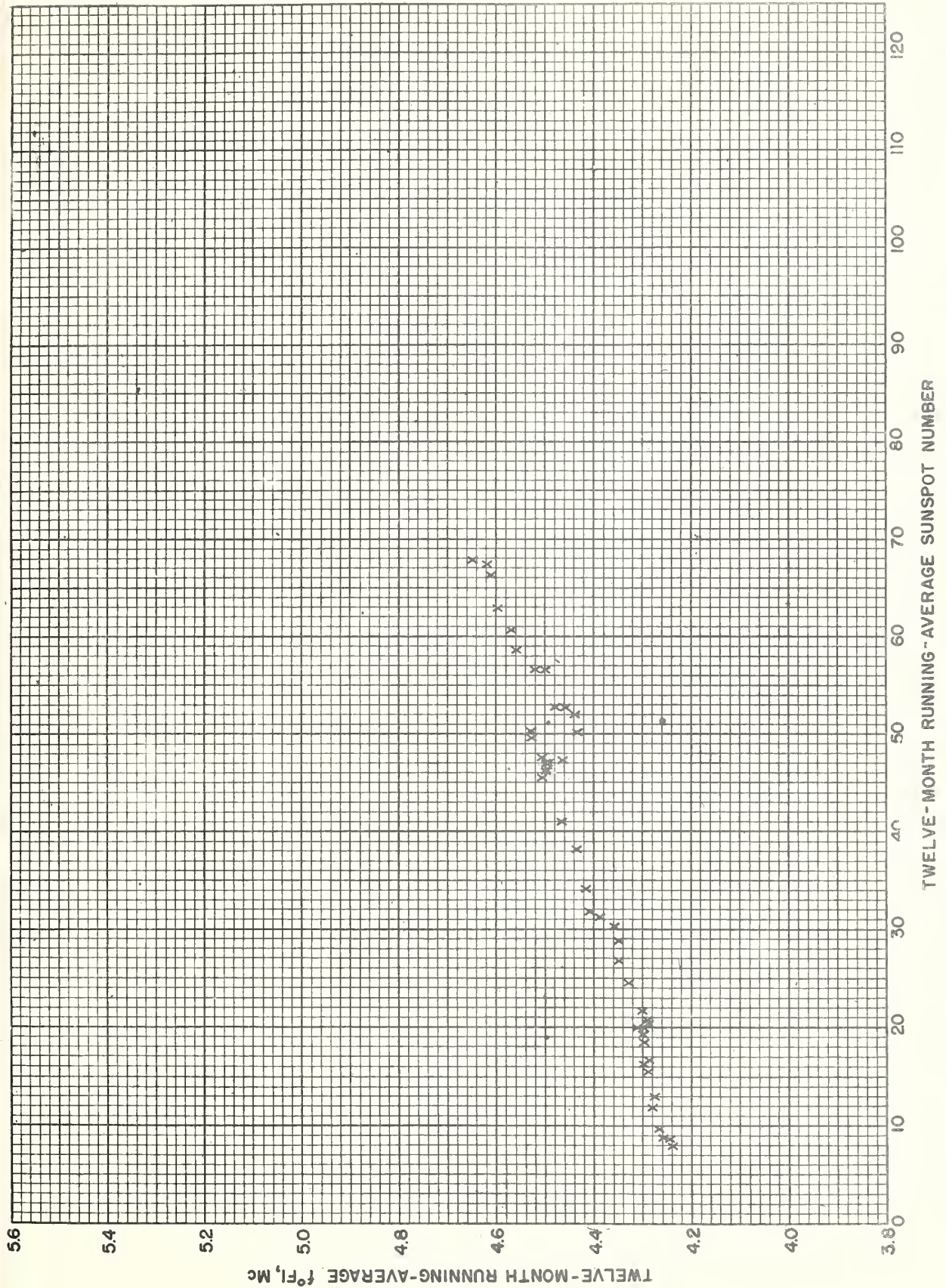


Fig. 7. VARIATION OF TWELVE-MONTH RUNNING-AVERAGE f°F1,1200, AT WASHINGTON, D.C., WITH TWELVE-MONTH RUNNING-AVERAGE SUNSPOT NUMBER.

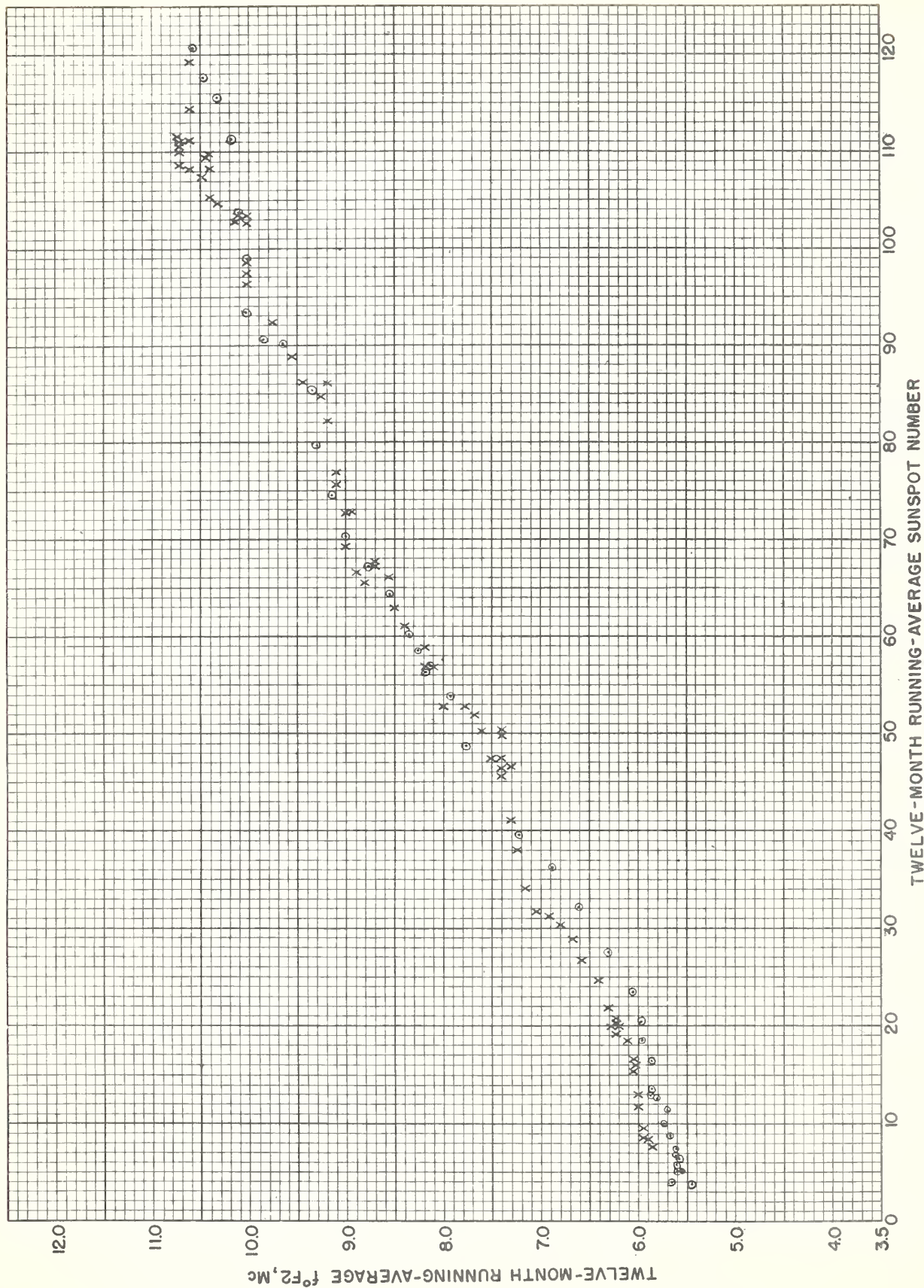


Fig. 8. VARIATION OF TWELVE-MONTH RUNNING-AVERAGE f°F2, 1200, AT WASHINGTON, D. C., WITH TWELVE-MONTH RUNNING-AVERAGE SUNSPOT NUMBER.

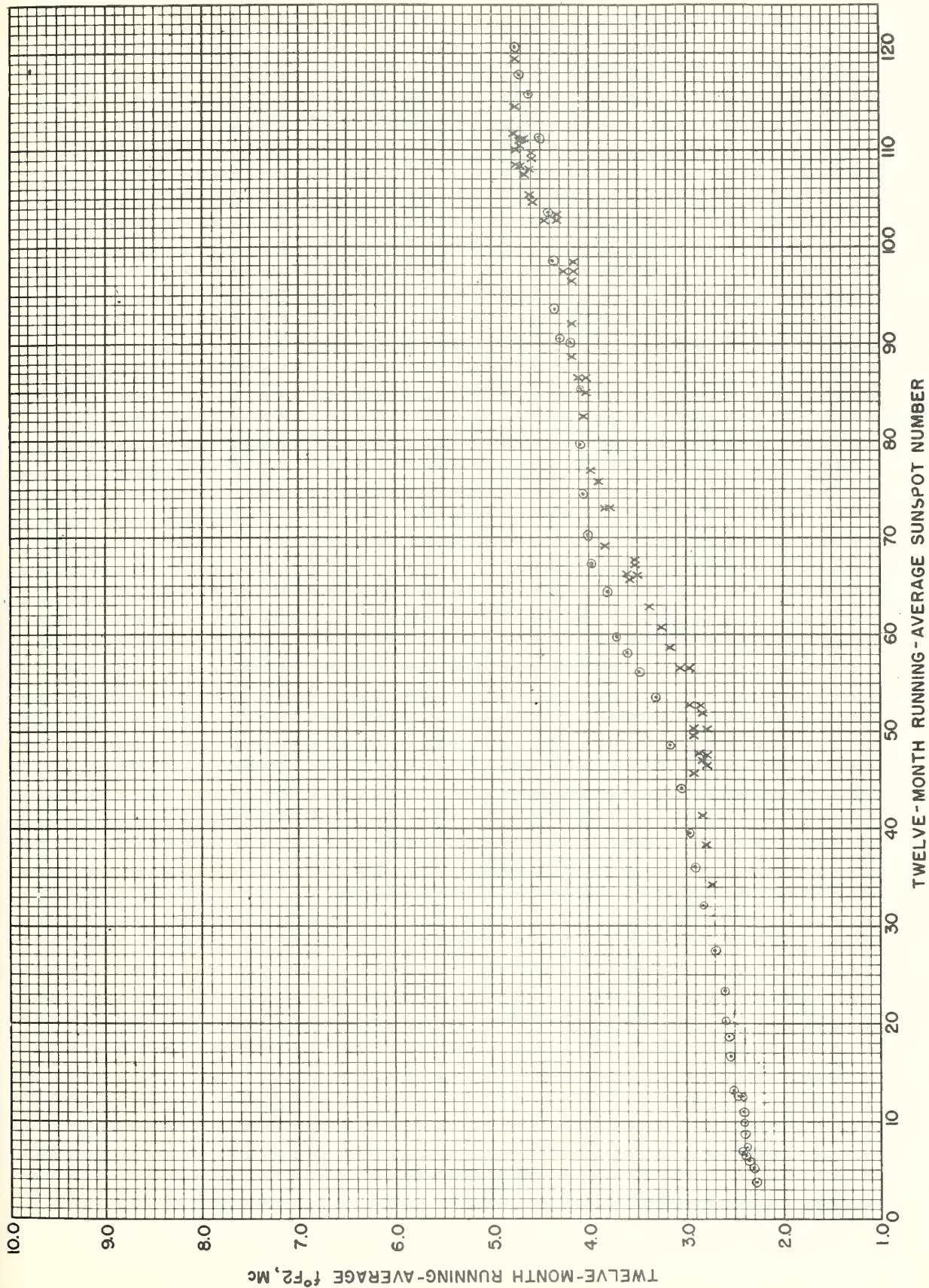
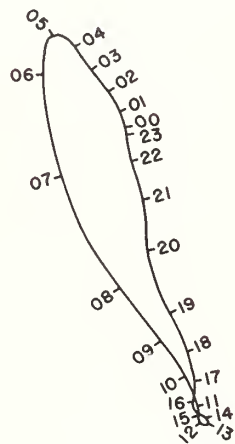


Fig. 9. VARIATION OF TWELVE-MONTH RUNNING-AVERAGE f°F2, PRE-SUNRISE MINIMUM, AT WASHINGTON, D.C., WITH TWELVE-MONTH RUNNING-AVERAGE SUNSPOT NUMBER.

YEARLY
AVERAGE
 $f^{\circ}F_2$,
Mc



TIME OF DAY,
75° W



SUNSPOT
NUMBER



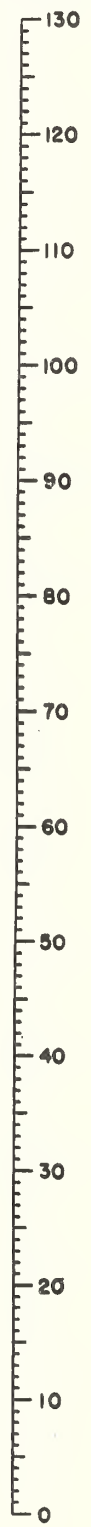
Fig.10.

NOMOGRAM FOR OBTAINING YEARLY AVERAGE $f^{\circ}F_2$ AT WASHINGTON, D. C.

YEARLY
AVERAGE
f°F2,
Mc



SUNSPOT
NUMBER



TIME OF DAY,
75° W

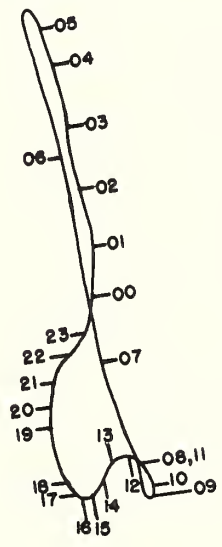


Fig.11.

NOMOGRAM FOR OBTAINING YEARLY AVERAGE f°F2 AT HUANCAYO, PERU

YEARLY
AVERAGE
f°F2,

Mc



SUNSPOT
NUMBER



TIME OF DAY,

120° E

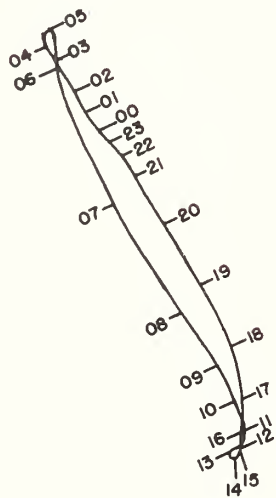


Fig.12.

NOMOGRAM FOR OBTAINING YEARLY AVERAGE f°F2, AT WATHEROO, W. AUSTRALIA

MONTHLY
AVERAGE
 $f^{\circ}F_2$,
Mc

SUNSPOT
NUMBER



TIME OF DAY,
75° W

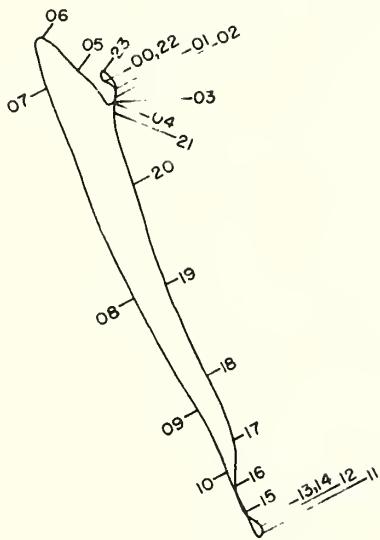


Fig.13.

NOMOGRAM FOR OBTAINING MONTHLY AVERAGE $f^{\circ}F_2$, JANUARY, AT WASHINGTON, D.C.

MONTHLY
AVERAGE
f°F2,
Mc

0
1
2
3
4
5
6
7
8
9
10
11
12
13
14
15

SUNSPOT
NUMBER

130
120
110
100
90
80
70
60
50
40
30
20
10
0

TIME OF DAY,

75° W

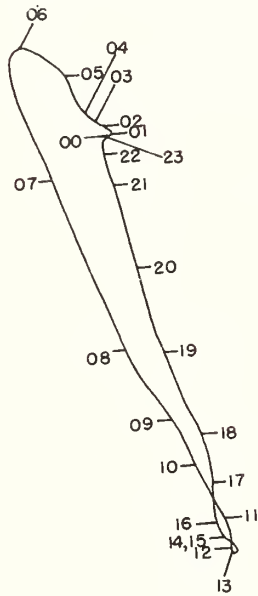


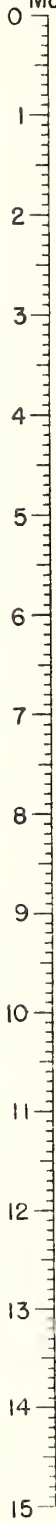
Fig. 14.

NOMOGRAM FOR OBTAINING MONTHLY AVERAGE f°F2, FEBRUARY, AT WASHINGTON, D.C.

MONTHLY
AVERAGE

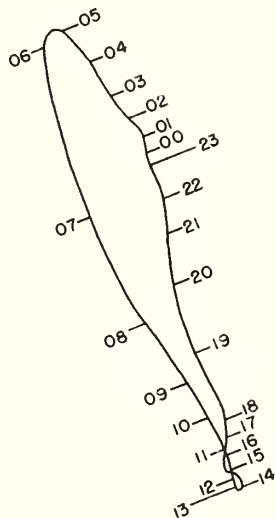
$f^{\circ}F_2$,

Mc



TIME OF DAY,

$75^{\circ} W$



SUNSPOT
NUMBER



Fig.15.

NOMOGRAM FOR OBTAINING MONTHLY AVERAGE $f^{\circ}F_2$, MARCH, AT WASHINGTON, D.C.



TIME OF DAY,
75° W

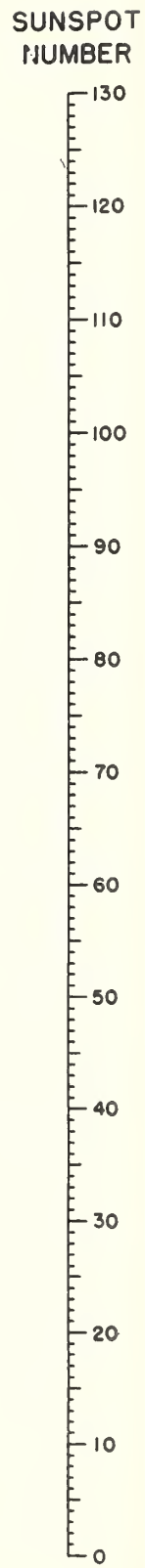
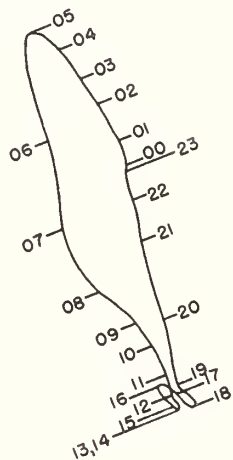


Fig.16.

NOMOGRAM FOR OBTAINING MONTHLY AVERAGE f° F2, APRIL, AT WASHINGTON, D.C.

MONTHLY
AVERAGE
f°F2,
Mc



SUNSPOT
NUMBER



TIME OF DAY,
75° W

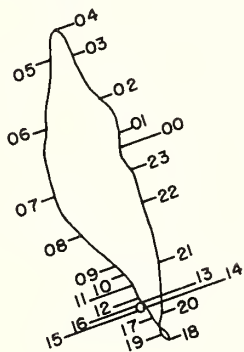


Fig.17.

NOMOGRAM FOR OBTAINING MONTHLY AVERAGE f°F2, MAY, AT WASHINGTON, D.C.

MONTHLY
AVERAGE
 $f^{\circ}F_2$,
Mc



SUNSPOT
NUMBER



TIME OF DAY,
75° W

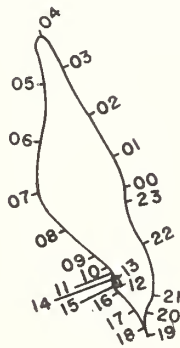


Fig.18.

NOMOGRAM FOR OBTAINING MONTHLY AVERAGE $f^{\circ}F_2$, JUNE, AT WASHINGTON, D.C.

MONTHLY
AVERAGE
f°F2,
Mc

0
1
2
3
4
5
6
7
8
9
10
11
12
13
14
15

SUNSPOT
NUMBER

130
120
110
100
90
80
70
60
50
40
30
20
10
0

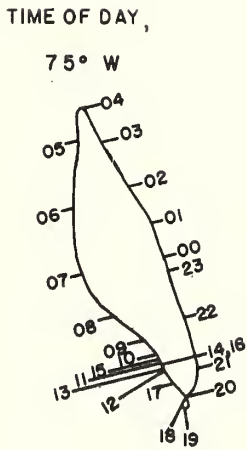


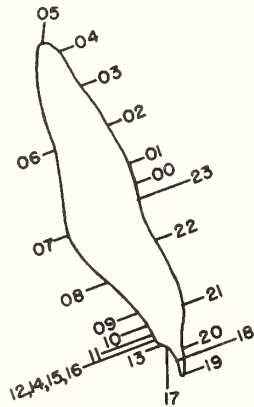
Fig.19.
NOMOGRAM FOR OBTAINING MONTHLY AVERAGE f°F2, JULY, AT WASHINGTON, D.C.

MONTHLY
AVERAGE

$f^{\circ}F_2$,
Mc



TIME OF DAY,
75° W



SUNSPOT
NUMBER



Fig 20.

NOMOGRAM FOR OBTAINING MONTHLY AVERAGE $f^{\circ}F_2$, AUGUST, AT WASHINGTON, D.C.

MONTHLY
AVERAGE
 $f^{\circ}F_2$,
Mc

SUNSPOT
NUMBER



TIME OF DAY,
75°W

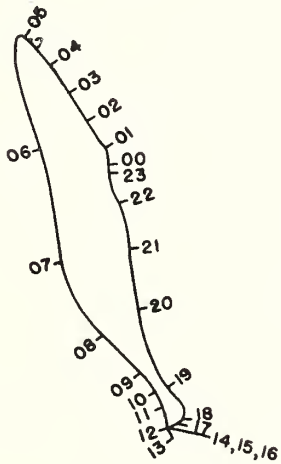


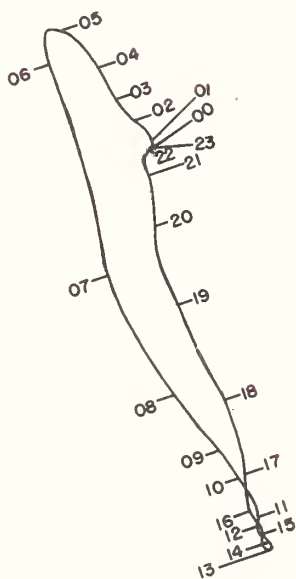
Fig.21.

NOMOGRAM FOR OBTAINING MONTHLY AVERAGE $f^{\circ}F_2$, SEPTEMBER, AT WASHINGTON, D.C.

MONTHLY
AVERAGE
f°F2,
Mc



TIME OF DAY,
75° W



SUNSPOT
NUMBER



Fig.22.

NOMOGRAM FOR OBTAINING MONTHLY AVERAGE f°F2, OCTOBER, AT WASHINGTON, D.C.



TIME OF DAY,
75° W

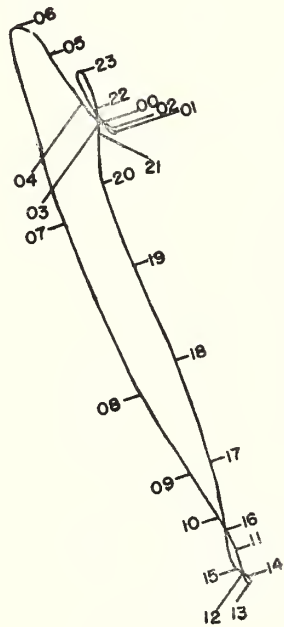


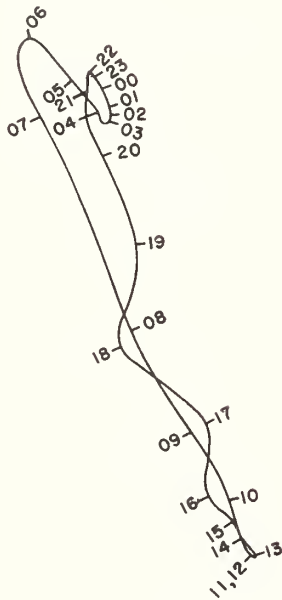
Fig.23.

NOMOGRAM FOR OBTAINING MONTHLY AVERAGE $f^{\circ}F_2$, NOVEMBER, AT WASHINGTON, D.C.

MONTHLY
AVERAGE
 $f^{\circ}F_2$,
Mc



TIME OF DAY,
75° W



SUNSPOT
NUMBER

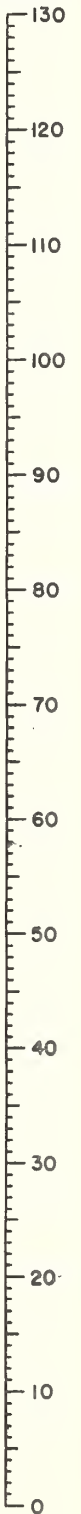
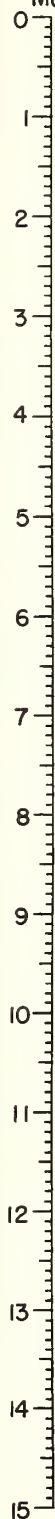


Fig.24

NOMOGRAM FOR OBTAINING MONTHLY AVERAGE $f^{\circ}F_2$, DECEMBER, AT WASHINGTON, D.C.

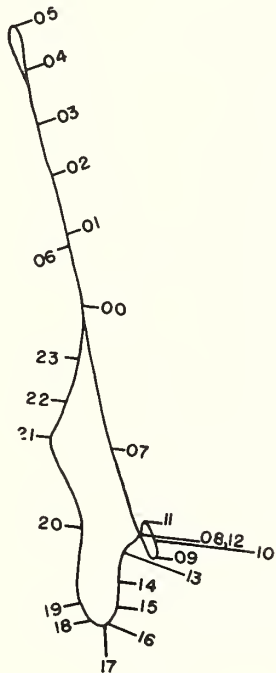
MONTHLY
AVERAGE

$f^{\circ}F_2$,
Mc



TIME OF DAY,

75° W



SUNSPOT
NUMBER

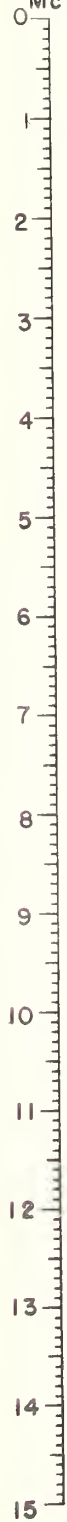


Fig. 25.

NOMOGRAM FOR OBTAINING MONTHLY AVERAGE $f^{\circ}F_2$, JANUARY, AT HUANCAYO, PERU

MONTHLY
AVERAGE
f° F2,

Mc



SUNSPOT
NUMBER



TIME OF DAY,

75° W

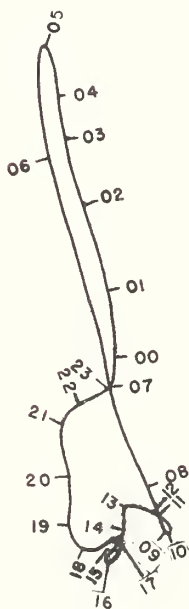
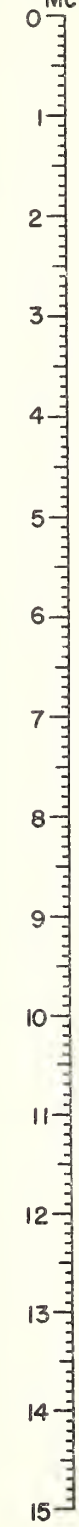


Fig.26.

NOMOGRAM FOR OBTAINING MONTHLY AVERAGE f° F2, FEBRUARY, AT HUANCAYO, PERU.

MONTHLY
AVERAGE
f°F2,
Mc



SUNSPOT
NUMBER



TIME OF DAY,

75° W

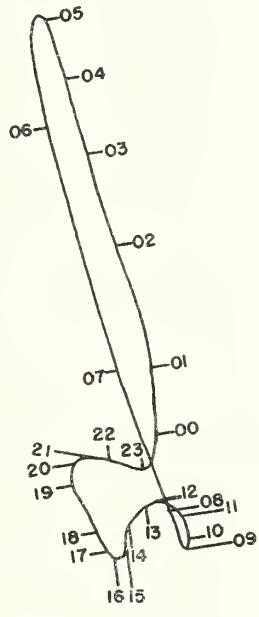


Fig 27

NOMOGRAM FOR OBTAINING MONTHLY AVERAGE f°F2, MARCH, AT HUANCAYO, PERU

MONTHLY
AVERAGE
f°F2,
Mc



SUNSPOT
NUMBER

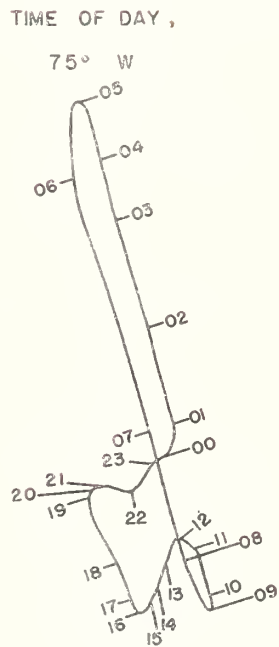


Fig. 28.

NOMOGRAM FOR OBTAINING MONTHLY AVERAGE f°F2, APRIL, AT HUANCAYO, PERU -

MONTHLY
AVERAGE

$f^{\circ}F_2$,
Mc



SUNSPOT
NUMBER



TIME OF DAY,

75° W

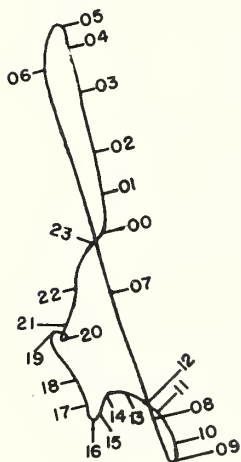


Fig.29.

NOMOGRAM FOR OBTAINING MONTHLY AVERAGE $f^{\circ}F_2$, MAY, AT HUANCAYO, PERU

MONTHLY
AVERAGE

$f^{\circ}F_2$,
Mc



SUNSPOT
NUMBER



TIME OF DAY,
75° W

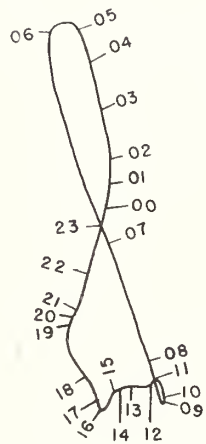


Fig. 30.

NOMOGRAM FOR OBTAINING MONTHLY AVERAGE $f^{\circ}F_2$, JUNE, AT HUANCAYO, PERU

MONTHLY
AVERAGE
 $f^{\circ}F_2$,
Mc

SUNSPOT
NUMBER

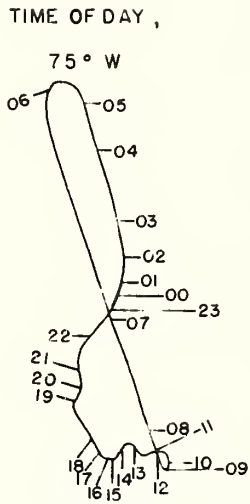
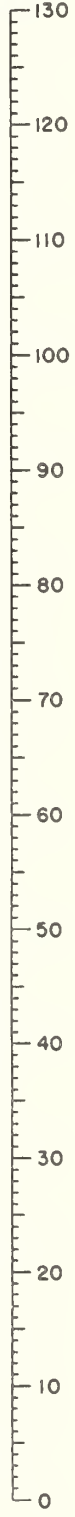


Fig.31.

NOMOGRAM FOR OBTAINING MONTHLY AVERAGE $f^{\circ}F_2$, JULY, AT HUANCAYO, PERU

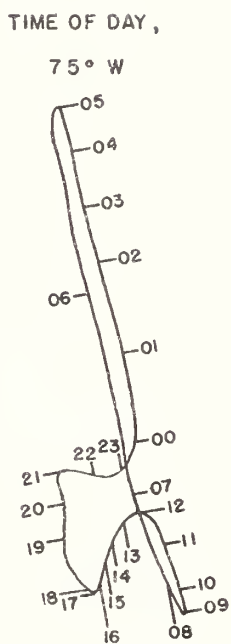
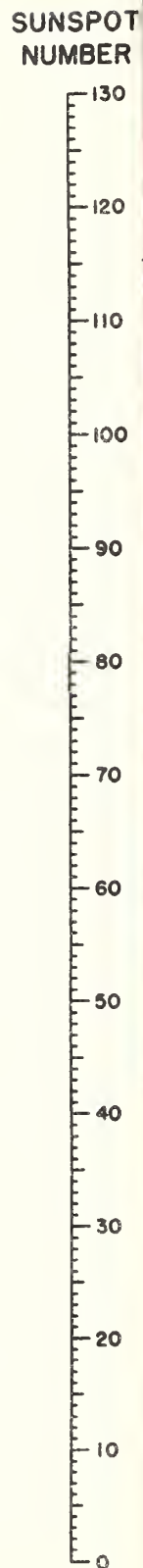


Fig.34.

NOMOGRAM FOR OBTAINING MONTHLY AVERAGE $f^{\circ}F2$, OCTOBER, AT HUANCAYO, PERU

POT
BER

MONTHLY
AVERAGE
 $f^{\circ}F_2$,
Mc

SUNSPOT
NUMBER



TIME OF DAY

75° W

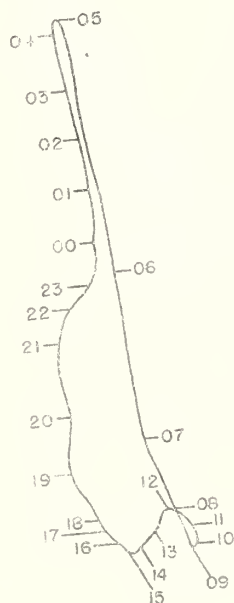


Fig 35.

NOMOGRAM FOR OBTAINING MONTHLY AVERAGE $f^{\circ}F_2$, NOVEMBER, AT HUANCAYO, PERU

MONTHLY
AVERAGE
f°F2,
Mc



SUNSPOT
NUMBER



TIME OF DAY,

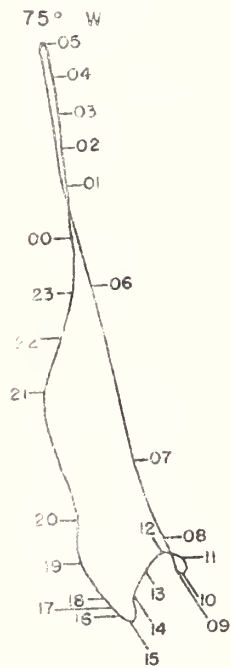


Fig.36.

NOMOGRAM FOR OBTAINING MONTHLY AVERAGE f°F2, DECEMBER, AT HUANCAYO, PERU

MONTHLY
AVERAGE
 $f^{\circ}F_2$,
Mc

SUNSPOT
NUMBER



TIME OF DAY,

120° E

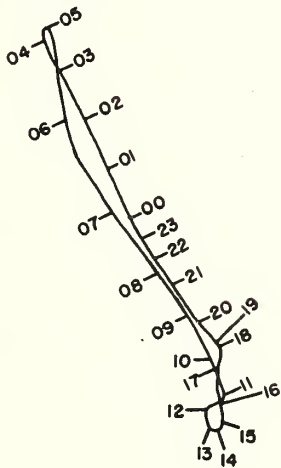


Fig.37

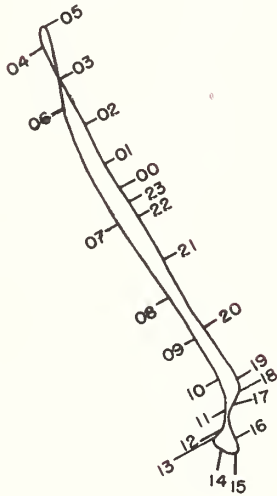
NOMOGRAM FOR OBTAINING MONTHLY AVERAGE $f^{\circ}F_2$, JANUARY, AT WATHEROO, W.AUSTRALIA

MONTHLY
AVERAGE
f°F2,
Mc



TIME OF DAY,

120° E



SUNSPOT
NUMBER



Fig. 38.

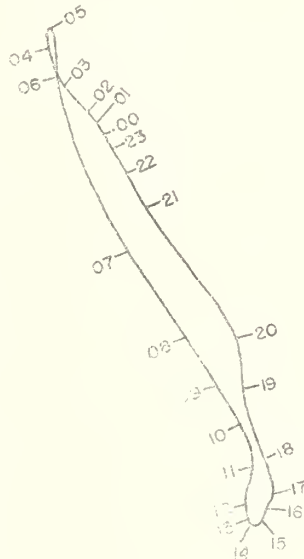
NOMOGRAM FOR OBTAINING MONTHLY AVERAGE f°F2, FEBRUARY, AT WATHEROO, W. AUSTRALIA

MONTHLY
AVERAGE
f°F2,
Mc



TIME OF DAY,

120° E



SUNSPOT
NUMBER



Fig.39.

NOMOGRAM FOR OBTAINING MONTHLY AVERAGE f°F2, MARCH, AT WATHEROC, W.AUSTRALIA

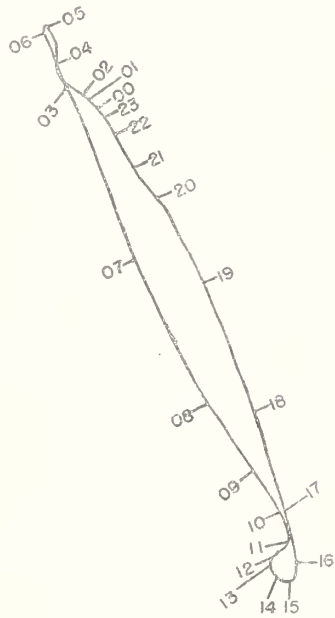
MONTHLY
AVERAGE

$f^{\circ}F_2$,

Mc



TIME OF DAY,
120° E



SUNSPOT
NUMBER



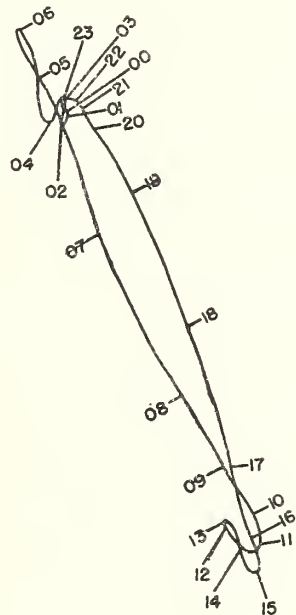
Fig.40.

NOMOGRAM FOR OBTAINING MONTHLY AVERAGE $f^{\circ}F_2$, APRIL, AT WATHEROO, W.AUSTRALIA

MONTHLY
AVERAGE
f°F2,
Mc



TIME OF DAY,
120° E



SUNSPOT
NUMBER



Fig. 41.

NOMOGRAM FOR OBTAINING MONTHLY AVERAGE f°F2, MAY, AT WATHEROO, W.AUSTRALIA

MONTHLY
AVERAGE
 $f^{\circ}F2$,
Mc

SUNSPOT
NUMBER



TIME OF DAY,
120° E

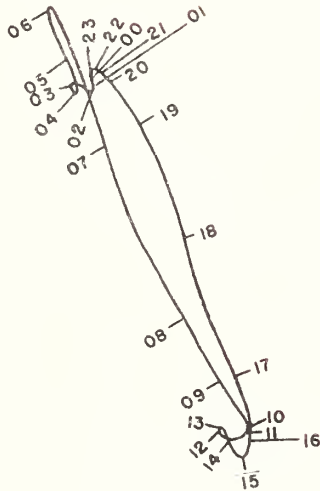


Fig.42.

NOMOGRAM FOR OBTAINING MONTHLY AVERAGE $f^{\circ}F2$, JUNE, AT WATHEROO, W. AUSTRALIA.

MONTHLY
AVERAGE
f°F2,
Mc

SUNSPOT
NUMBER



TIME OF DAY,
120° E

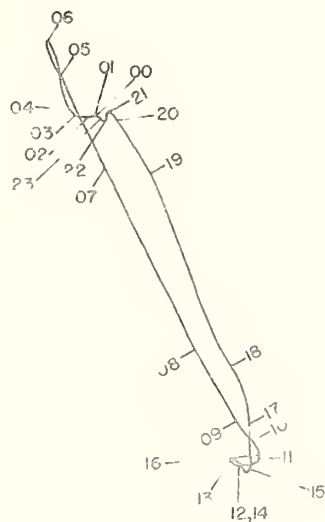


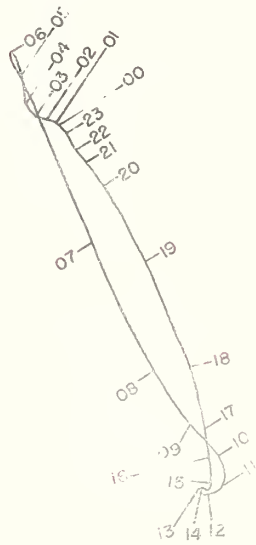
Fig.43.

NOMOGRAM FOR OBTAINING MONTHLY AVERAGE f°F2, JULY, AT WATHEROO, W. AUSTRALIA

MONTHLY
AVERAGE
f°F2,
Mc



TIME OF DAY,
120° E



SUNSPOT
NUMBER



Fig.44.

NOMOGRAM FOR OBTAINING MONTHLY AVERAGE f°F2, AUGUST, AT WATHEROC, WAUSTRALIA

MONTHLY
AVERAGE
 $f^{\circ}F_2$,



SUNSPOT
NUMBER



TIME OF DAY,
120° E

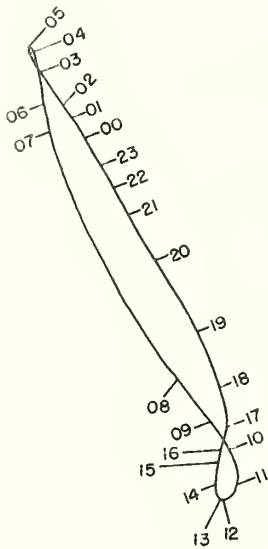
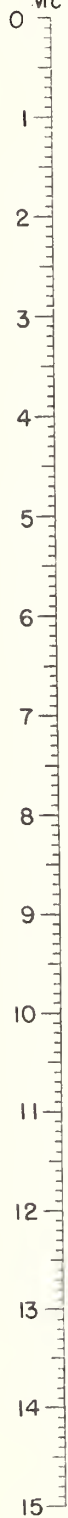


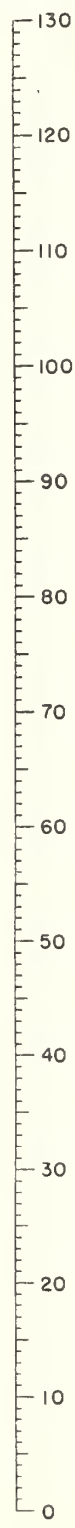
Fig.45.

NOMOGRAM FOR OBTAINING MONTHLY AVERAGE $f^{\circ}F_2$, SEPTEMBER, AT WATHEROO, W.AUSTRALIA

MONTHLY
AVERAGE
f°F2,
Mc



SUNSPOT
NUMBER



TIME OF DAY.
120° E

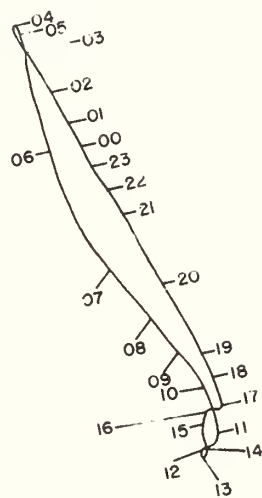


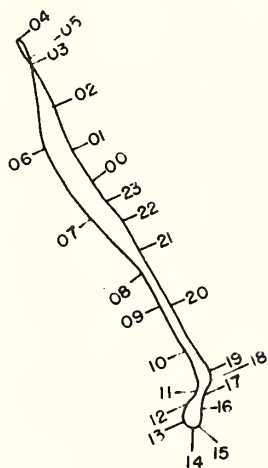
Fig.46.

NOMOGRAM FOR OBTAINING MONTHLY AVERAGE f°F2, OCTOBER, AT WATHEROO, W.AUSTRALIA

MONTHLY
AVERAGE
 $f^{\circ}F_2$,
Mc



TIME OF DAY,
120° E



SUNSPOT
NUMBER



Fig.47.

NOMOGRAM FOR OBTAINING MONTHLY AVERAGE $f^{\circ}F_2$, NOVEMBER, AT WATHEROO, W.AUSTRALIA

MONTHLY
AVERAGE

$f^{\circ}F_2$

Mc



SUNSPOT
NUMBER



TIME OF DAY,
120° E

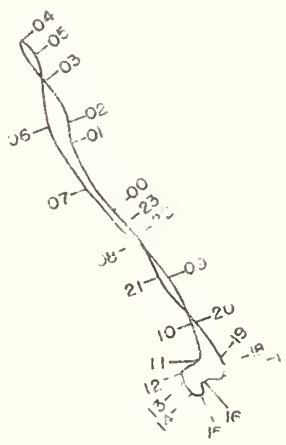


Fig.48.

NOMOGRAM FOR OBTAINING MONTHLY AVERAGE $f^{\circ}F_2$, DECEMBER, AT WATHEROO, WAUSTRALIA

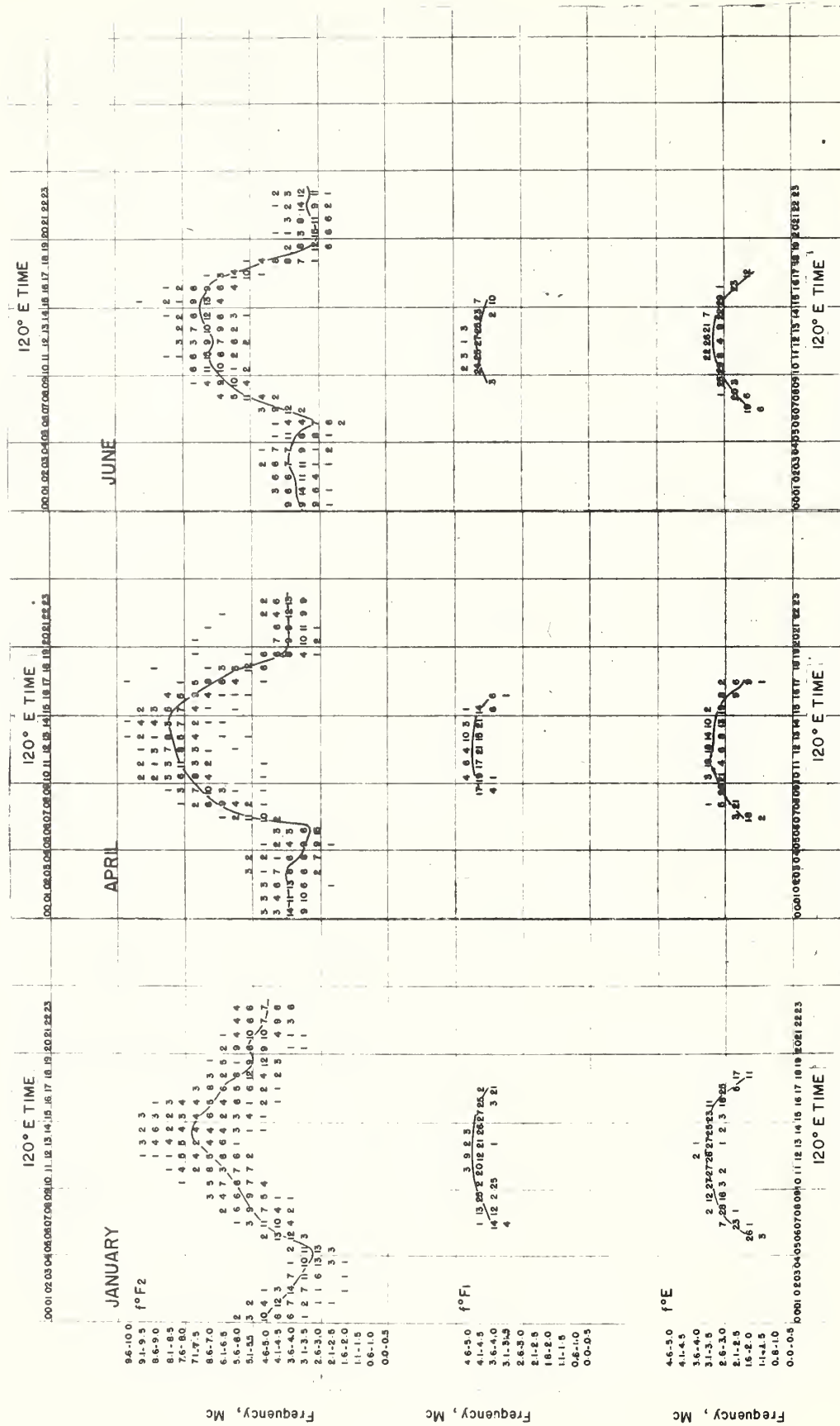


Fig. 50. DISTRIBUTION OF CRITICAL FREQUENCIES DURING JANUARY, APRIL, AND JUNE, 1945, AT WATHEROO, W. AUSTRALIA. NUMBERS REFER TO NUMBER OF CASES LYING BETWEEN INDICATED BAND LIMITS CURVES INDICATE MONTHLY MEDIAN VALUES.

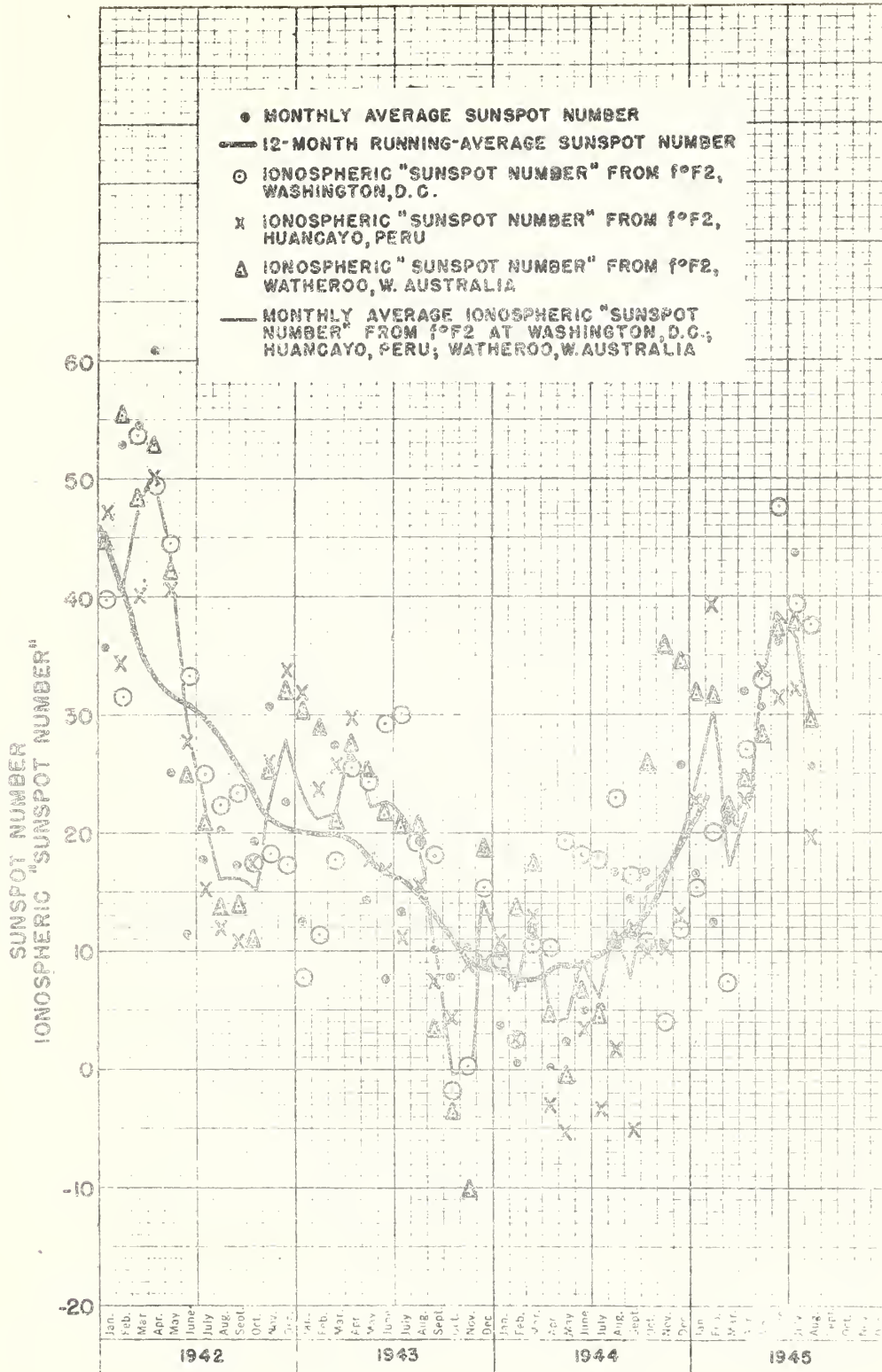


Fig.51. COMPARISON OF RELATIVE SUNSPOT NUMBER AND IONOSPHERIC "SUNSPOT NUMBER" AS DERIVED FROM f²F2 VALUES OBSERVED BETWEEN 1000 AND 1400, APPROXIMATE LOCAL TIME, AT WASHINGTON, D.C., HUANCAYO, PERU, AND WATHEROO, W. AUSTRALIA.

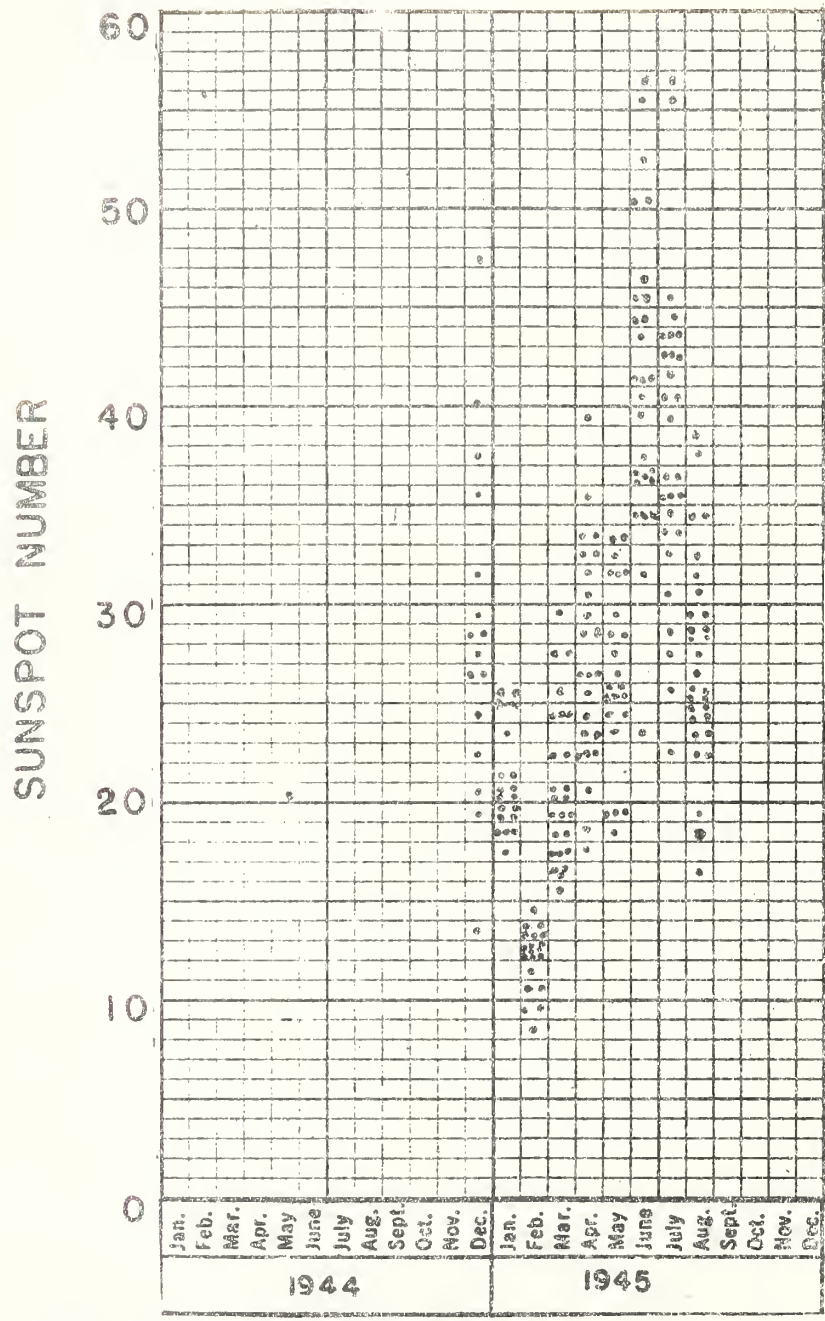


Fig. 52. VARIATION IN MONTHLY AVERAGE
 RELATIVE SUNSPOT NUMBERS FROM
 AMERICAN OBSERVERS

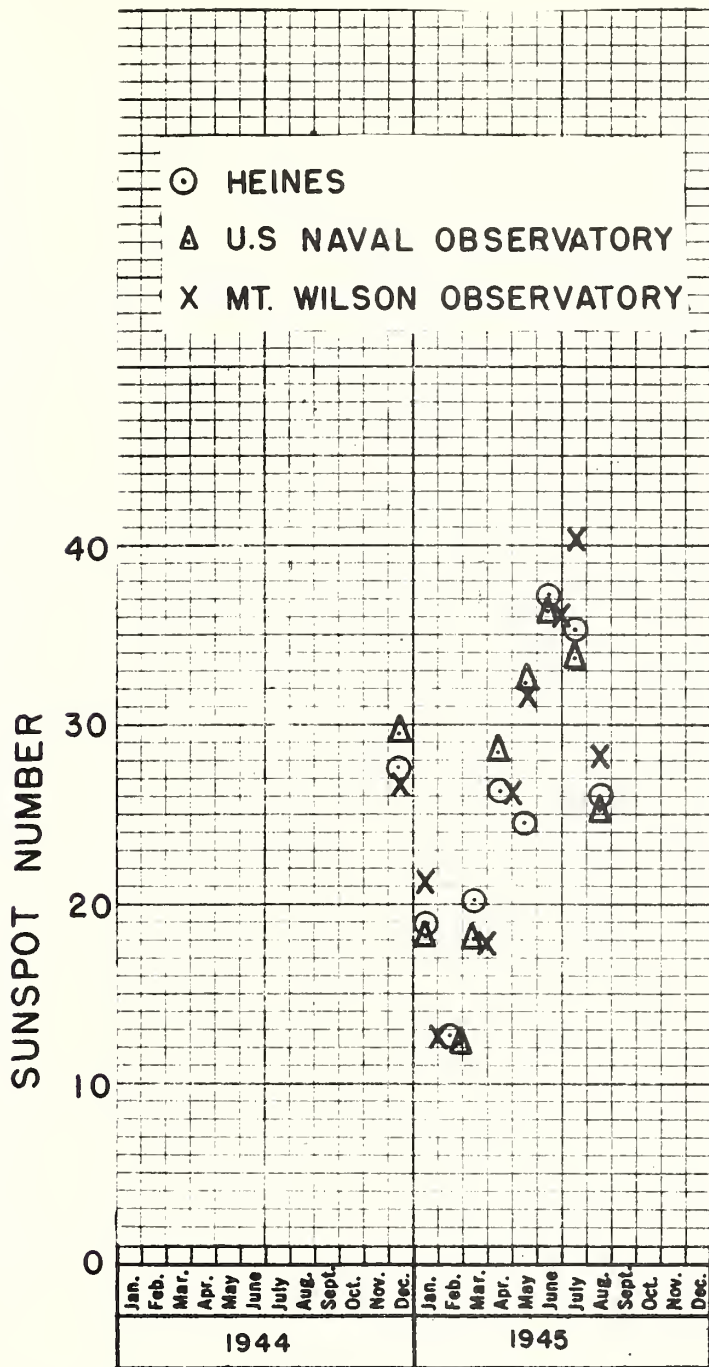


Fig. 53. VARIATION IN MONTHLY AVERAGE
 RELATIVE SUNSPOT NUMBERS,
 HEINES, U.S. NAVAL OBSERVATORY,
 MT. WILSON OBSERVATORY.

